EREM 80/2
Journal of Environmental Research, Engineering and Management
Vol. 80 / No. 2 / 2024
pp. 24–38
10.5755/j01.erem.80.2.35898

NaOH-Activated Tofu Waste Adsorbent for Pb(II) and Cu(II) Adsorption: Kinetic and Isotherm Studies

Received 2023/12 | Accepted after revisions 2024/04

https://doi.org/10.5755/j01.erem.80.2.35898

NaOH-Activated Tofu Waste Adsorbent for Pb(II) and Cu(II) Adsorption: Kinetic and Isotherm Studies

Rita Sunartaty[1,2], Abrar Muslim[1]*, Sri Aprilia[1], Mahidin[1]

[1] Postgraduate School of Engineering Studies, Universitas Syiah Kuala, Darussalam, Indonesia

[2] Department of Agricultural Industrial Engineering, Faculty of Agricultural Technology, Universitas Serambi Mekkah, Indonesia

***Corresponding author:** abrar.muslim@usk.ac.id

The study was focused on developing adsorbents from tofu waste (TW) for the adsorption of Pb(II) and Cu(II). FTIR analysis showed that NaOH activation of TW affected the transmittance of active sites. XRD analysis identified increasing crystallinity after NaOH treatment. SEM analysis demonstrated larger pores with higher NaOH concentrations, reducing adsorbent size. The adsorption capacity reached a maximum equilibrium of 99.86 mg/g and 87.81 mg/g for Pb(II) and Cu(II), respectively, using TW activated by 0.6 M NaOH. Both Pb(II) and Cu(II) adsorptions followed a linearized pseudo second-order kinetics model, with capacities of 100.00 mg/g and 87.719 mg/g, respectively. The Langmuir isotherm provided the best fit, yielding maximum overall adsorption capacities of 77.519 mg/g for Pb(II) and 91.743 mg/g for Cu(II) at the initial concentrations being 9.89–499.51 mg/L and 10.08–499.92 mg/L for Pb(II) and Cu(II), respectively. Brunauer–Emmett–Teller study results showed that the saturation capacities and total pore volumes were 50.505 mg/g and 49.500 L/mg, respectively, for Pb(II), and 84.388 mg/g and 237.000 L/mg, respectively, for Cu(II).

Keywords: adsorption, heavy metal removal, tofu waste adsorbent, kinetic, isotherm, Brunauer–Emmett–Teller.

Introduction

Increasing industrial activities have led to an increase in heavy metals in wastewater. Water pollution caused by heavy metal ions has become a major environmental problem in some developing countries. Heavy metal pollution can decrease the quality of an ecosystem. Heavy metal ions can cause human health problems because their pollution is persistent, long-term and covert (Ali et al., 2019). Because heavy metals cannot be naturally degraded, they can accumulate in the human body throughout the food chain (Khan et al., 2015).

Among other heavy metals, Pb(II) and Cu(II) have become a major concern in various developing countries due to the increasing industrial activities. Pb(II), which is a non-biodegradable pollutant, can be released to water bodies from industrial activities including agricultural and mining practices (Yan-Bao et al., 2013). Accumulating this hazardous Pb(II) in the human body can cause respiratory, urinary, cardiovascular, digestive and neurologic diseases (Ebrahimi et al., 2020). Meanwhile, copper is a widely used heavy metal, and its mine plants in the world have a 10 times higher capacity compared with other non-ferrous metals (Milićević et al., 2020). Cu(II) ions can be released to surface water from agricultural, chemical and electrical industries, petroleum and mining operation, and even households(Biswajit and Sudip, 2013). Its redox activity in the human body can cause tumors and cancer (Lelièvre et al., 2020) and neurological diseases due to various organ disorders (Jomova et al., 2022). The maximum contaminant level (MCL) of Pb(II) and Cu(II) in drinking water required by the Environmental Protection Agency (EPA) is 0.015 mg/L and 1.3 mg/L, respectively (Griffiths et al., 2021). Therefore, decreasing and removing Pb(II) and Cu(II) in contaminated wastewater before discharging it to the environment are necessary to protect human beings.

Several methods have been proposed for many years to reduce the concentration of heavy metal ions, including Pb(II) and Cu(II), from wastewater; however, attaining the most economical and effective method is still challenging to conduct. Physical and chemical processes include precipitation, reverse osmosis, solvents (Kurniawan et al., 2006), oxidation based on photo-Fenton and electrochemical degradation (Vorontsov, 2019; Mansouri et al., 2019; Jiménez et al., 2019), sedimentation by flocculation (Lee et al., 2008; Inam et al., 2019), ion-exchange (Fu and Wang, 2011), and membrane filtration (Quist-Jensen et al., 2015). Among physical and chemical processes, various adsorption approaches have been widely used due to their cost-effectiveness, easy operational conditions and simplicity regeneration (Geng et al., 2012; Samiey et al., 2014; Wang et al., 2014).

Various organic adsorbents derived from agricultural solid wastes have been employed in the adsorption of Cu(II), such as those derived from cocoa cortex (Fotsing et al., 2020), green vegetable waste (Sabela et al., 2019), coconut cake, groundnut seed and sesame seed (Kumar et al., 2019), fermented corn stalk (Ren et al., 2018), and palm oil fruit shells (Hossain et al., 2012). The organic adsorbents utilized from coconut fibers, rice husk and moringa leaves (Dharsana and Josej, 2020), oryza sativa husk (Kaur et al., 2020), cucumber peel (Basu et al., 2017), tomato waste (Yargic et al., 2015), olive tree pruning waste (Blázquez et al., 2011), and heartwood of areca catechu powder (Chakravarty et al., 2010) have been applied for Pb(II) adsorption.

The amount of tofu waste was predicted to be approximately 14 million tonnes every year (Mok et al., 2019), and it was projected to increase by 5.2% through 2019 to 2029 following the tofu market growth by 5.2% (Grand View Research, 2019; Maximize Market Research, 2023). Tofu waste is well-known as soybean waste, limbah ampas tahu (Indonesian), Okara or tofukasu (Japanese), tauhu tor (Thai) and doufuzha (Chinese). It contains approximately 25% of protein, 50% of fiber, 10% of lipid and other high-value compounds such as lignins, isoflavones, saponins, etc. (Mok et al., 2019). Protein surface is covered by functional active sites including alcohol, hydroxyl, carbonyl, amino acids, ester, amine and carboxyl, which can bind metal ions (Kampalanonwat and Supaphol, 2014). Dried tofu waste was used for the adsorption of Cr(III), and the maximum adsorption capacity determined was 4.498 mg/g at 160 min of contact time (Perwitasari, 2021). Tofu waste without chemical activation was used as adsorbent for Cu(II) and Pb(II), and the maximum adsorption capacity was obtained to be 7.55 mg/g and 7.90 mg/g, respectively. The functional groups are alcoholic, amino, carbonyl, etc., and they have affinity for the adsorption of heavy metal ions (Dancila et al., 2019).

NaOH activators affect the surface characteristics of an adsorbent (Hafizuddin et al., 2021) and increase its total surface area (Andre et al., 2011). NaOH concentration also affects the adsorption capacity of heavy metal, increasing the adsorption capacity of Pb(II) by activated Areca Catechu shell (Muslim et al., 2017), and it can increase the adsorption of Cu(II) by the adsorbent from Musa Acuminata Banana Bunch (Muslim et al., 2021). The amount of metal ions present on the adsorbent, commonly referred to as adsorption capacity, can be varied with contact time. This relationship could be a linear increase in 40 min, and a sudden linear decrease for the rest of the time, i.e., 50 min (Ifijen et al., 2020), an exponential increase with a 200-min equilibrium time (Li et al., 2022) and a 60-min equilibrium time (Muslim et al., 2022), and dynamic two stages of

fluctuations reaching an equilibrium in 120 min (Kazmierczak et al., 2021).

The adsorption equilibrium can be achieved within a reasonable timeframe. The rate of adsorption and the equilibrium adsorption capacity can be determined using adsorption kinetic models (Mashhadimoslem et al., 2024). The Lagergren and Ho adsorption kinetic models are commonly utilized due to their ability to describe the adsorption process and offer valuable insights into the adsorption mechanism (Revellame et al., 2020). Moreover, these models are relatively straightforward to apply (Al-Harby et al., 2021). To ascertain the overall adsorption capacity, adsorption equilibrium may be evaluated across various initial concentrations of adsorbate in the solution (Obulapuram et al., 2021). The Freundlich and Langmuir isotherm models are widely employed to predict the overall adsorption capacity across varying amounts of adsorbate at a constant temperature (Khayyun and Mseer, 2019). Additionally, the Brunauer-Emmett-Teller (BET) model is reliable for determining the total pore volume and adsorption isotherm capacity (Murphy et al., 2023).

The main objective of this study was to provide valuable insights into the effects of NaOH reagent for activating tofu waste on the properties of tofu waste (TW) related to the TW functional active sites and physical morphology throughout Fourier-transform infrared spectroscopy (FTIR), structural equation modelling (SEM), and X-ray diffraction (XRD) analysis. The effect of contact time and NaOH concentration on the adsorptions of Cu(II) and Pb(II) were examined. Adsorption kinetic and isotherms studies were carried out to obtain the related constants by fitting the adsorption test data to the linearized models of adsorption kinetic and isotherms. The effect of NaOH concentration on the kinetic and isotherm constants was evaluated, including isotherm-based Brunauer–Emmett–Teller model.

Materials and Methods

The TW adsorbent without chemical activation

The fresh TW samples were obtained from the waste generated by a tofu company in Lamteumen Barat Village, Banda Aceh. The fresh TW sample of 2 kg was washed thoroughly with reverse osmosis water until residual milk was removed. It was then rinsed with distillate water, and pressed to reduce the water. To remove the rest water and bound moisture, it was dried at 105°C (± 1°C) in an oven (Memmert NN-ST342M, Western Germany) until reaching a constant final mass. The dried TW of 1 kg was ground into powder and sieved (ASTM standard) to 60–100 mesh size to get a stock of TW powder. The TW powder of 30 g was separated, stored in a sealed bottle, and labelled as TW (TW adsorbent without chemical activation).

The TW adsorbent with chemical activation

To prepare the activated TW adsorbent, 30 g of TW powder was taken from the stock. Chemical activation of the TW powder was conducted by contacting 30 g of TW powder with 200 mL of NaOH solution at 0.2 M in a beaker glass, which was stirred at 100-rpm and 30°C (± 1°C) using a magnetic stirrer for 24 h (Muslim et al., 2022). The pH of the activated TW adsorbent was neutralized by washing it many times using distilled water and filtering using vacuum filter. The activated TW was dried at 105°C (± 1°C) in the oven until reaching a constant final mass. This activated TW adsorbent was stored in a sealed bottle and labelled as TW 0.2 (TW adsorbent activated using 0.2 M NaOH). This chemical activation procedure was repeated for another 30 g of TW powder using 0.4 M NaOH to produce TW 0.4. The above procedure was also repeated for another 30 g of TW powder using 0.6 M NaOH to produce TW 0.6. The operation condition of TW chemical activation is listed in *Table 1*.

Table 1. *Operation condition of TW chemical activation*

Type of adsorbent			
Activation conditions	TW 0.2	TW 0.4	TW 0.6
NaOH solution concentration	0.2 M	0.4 M	0.6 M
NaOH solution volume	200 mL	200 mL	200 mL
TW powder mass	30 g	30 g	30 g
Temperature of activation	30 °C (± 1°C)	30 °C (± 1°C)	30 °C (± 1°C)
Temperature of drying	105°C (± 1°C)	105°C (± 1°C)	105°C (± 1°C)

Characterization of TW adsorbents

The functional groups of TW, TW 0.2, TW 0.4 and TW 0.6 were analysed with FTIR (Shimadzu Prestige 21, Japan). The KBr Pellet method was used. Each sample

of 0.5 mg was finely pulverized to mix the sample with 500 mg of KBr, and the mixture was dried at 110°C (± 1°C) in the oven. The spectra of samples were quantified at the range of 400–4000 cm^{-1} of wavenumber. To determine the crystal structure of the samples, XRD (Shimadzu 7000, Japan) was used, and the observation of the scattered intensity begins at a diffraction angle of θ = 0° and continues up to 60°. SEM (HITACHI TM3000, Japan) was employed to observe the sample surface characteristics under 50/60Hz and phase 1 of 500VA. Prior to SEM examination, all samples underwent a drying process at 105°C for 20 min in the oven (Muslim et al., 2022).

Experiments of Pb(II) and Cu(II) adsorption

All adsorption experiments were conducted in a batch mode at standard pH, atmospheric pressure, and room temperature. The experimental procedure followed that of the previous study (Muslim et al., 2021). A mass of 0.5 g of TW was brought into contact with 100 mL of Pb(II) aqueous solution with a predetermined initial concentration of 499.51 mg/L, and the TW-solution system was stirred at 100 rpm. Pb(II) concentration in the solution after adsorption at intervals of 10, 20, 30, 40, 50, and 60 minutes was determined by extracting 1 mL of the filtrate sample at each time point, which was then mixed with 11 mL of distilled water. Analysis was conducted using atomic absorption spectroscopy (AAS), with the real Pb(II) concentration determined by a dilution factor of 12. This experimental procedure was repeated for initial Pb(II) concentrations of 9.89, 25.20, 48.90, 124.56, and 248.60 mg/L, as well as for a TW-solution with a mass of 0.6 g. Equilibrium time was determined based on both adsorption experiments and used to calculate the adsorption capacity of TW 0.2 and TW 0.4. To assess the effect of NaOH concentration, the adsorption capacity of each adsorbent was determined at equilibrium. All experiments for Pb(II) adsorption were repeated for Cu(II) adsorption, with initial Cu(II) concentrations set at 10.08, 24.40, 50.08, 124.70, 249.05, and 499.92 mg/L. The difference in initial Cu(II) concentration compared with Pb(II) was due to distinct AAS analyses.

Measuring adsorption capacity across time

The adsorption capacity for Pb(II) and Cu(II) was assessed by applying *Equation (1)* to the time series data of the respective heavy metal ions. This equation has been adapted from the prior study conducted by Nguyen and Pham (Nguyen and Pham, 2023):

$$q_t = \frac{(C_0 - C_t)V_{St}}{m_{AC}} \quad (1)$$

Where: C_0 (mg/L) is the concentration of heavy metal ions in aqueous solution at time t = 0 min, which is also noticed as the initial concentration of heavy metal ions; C_t (mg/L) is the concentration of heavy metal ions in aqueous solution at time t min; q_t (mg/g) represents the adsorption capacity at time t min; V_{St} (L) is solution volume at the time t; m_{AC} (g) denotes as mass of adsorbent.

Measuring adsorption kinetic

The linearized pseudo first-order kinetics (LPFOK) model (Lagergren, 1989) and the linearized pseudo second-order kinetics (LPSOK) model (Ho et al., 1996) were used to measure the adsorption kinetic of Pb(II) and Cu(II), and given as *Equations (2)* and *(3)*, respectively (Muslim, et al. 2017):

$$\log(q_e - q_t) = \log q_e - \left(\frac{k_L t}{2.303}\right) \quad (2)$$

$$\frac{t}{q_t} = \frac{1}{k_H q_e^{\,2}} + \frac{t}{q_e} \quad (3)$$

Where: k_L (/min) stands for the LPFOK adsorption rate constant; k_H (g/mg.min) represents the LPSOK adsorption rate constant; q_e (mg/g) is the adsorption capacity at equilibrium time.

Measuring adsorption isotherm

The linearized Langmuir adsorption isotherm (LLAI) model (Langmuir, 1918) and linearized Freundlich adsorption isotherm (LFAI) model (Freundlich, 1906) were used to measure the adsorption isotherm of Pb(II) and Cu(II), and given as *Equations (4)* and *(5)*, respectively (Syahiddin and Muslim, 2018):

$$\frac{C_e}{q_e} = \frac{1}{q_m K_L} + \frac{1}{q_m} C_e \quad (4)$$

$$\log q_e = \frac{1}{n}\log C_e + \log K_F \quad (5)$$

Where: C_e (mg/L) is the concentration of heavy metal ions in the aqueous solution at equilibrium; q_m (mg/g) signifies the adsorption capacity based on LLAI model; K_L (L/mg) is the pores volume of LLAI model; K_F (L/mg) indicates the pore volume of LFAI model; $1/n$ denotes the adsorption intensity.

The total pore volume and capacity of adsorption isotherms can be worked out using the linearized Brunauer–Emmett–Teller (BET) adsorption isotherm model (LBETAI model, Foo and Hameed, 2010):

$$\frac{C_e}{q_e(C_s - C_e)} = \frac{1}{q_s C_{BET}} + \frac{(C_{BET} - 1)}{q_s C_{BET}}\left(\frac{C_e}{C_s}\right) \quad (6)$$

Where: C_{BET} (L/mg) is the BET total pore volume; q_s (g/mg) is the BET saturation capacity; C_s (mg/L) is adsorbate saturation concentration.

Results and Discussion

FTIR spectroscopy analysis

The q_e of TW, TW 0.2 M, TW 0.4 M, and TW 0.6 M might be influenced by the presence of functional groups on the adsorbent. These groups can be detected using an FTIR spectrum. As can be seen by the FTIR spectra of TW 0.6 in *Fig. 2*, a wide band with a peak at 3277 cm^{-1} and a trasmittance of 42.8% corresponds to the O-H stretching vibration of the hydroxyl group in lignin, cellulose and hemicellulose at 3200–3500 cm^{-1} (Yu and Yang 2019; Zein et al., 2014, Hesas et al., 2013; Popescu et al., 2009) which illustrates the inherent hydrophilic nature of the fibers (Mondragon et al., 2014). The band representing the N-H stretching vibration of the peptide bond (-CO-NH-) can be observed at 3270–3310 cm^{-1} (Foggia et al., 2011).

Fig. 1. *The FTIR spectra for (a) TW, (b) TW 0.2, (c) TW 0.4 and (d) TW 0.6*

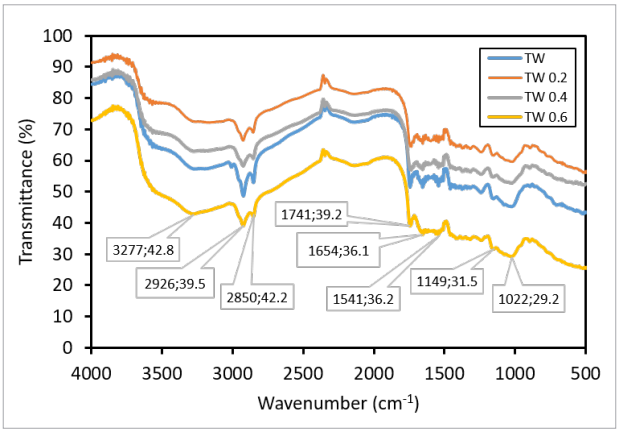

Various functional groups were also determined to be associated with specific peaks. The stretching of the C-H alkyl groups of celluloses (Yang et al., 2019; Fahma et al., 2011), or the CH_2 asymmetric stretching of lipid (Kumar et al., 2016), was identified at 2926 cm^{-1} with a trasmittance of 39.5%. The symmetric stretching vibration of -CH_2 was at 2850 cm^{-1} with a trasmittance of 42.2% (Sha et al., 2019). The peak at 1741 cm^{-1} with a trasmittance of 39.2% was attributed to C=O stretching of hemicelluloic ester groups of (Ullah et al., 2017; Fahma et al., 2011). The peaks at 1654 cm^{-1} with a trasmittance of 36.1% were linked to the C=O stretching of amide I (Skoog et al., 1998; Bentley) and the N-H stretching of proteins (Xiang et al., 2016) originating from the amide II band at 1541 cm^{-1} with a transmittance of 36.2% (Yang et al., 2019). Finally, the peaks at 1149 cm^{-1} and 1022 cm^{-1} with the transmittances of 31.5% and 29.2%, respectively, were assigned to the C-O group stretching of carbohydrates and lignin (Ullah et al., 2017; Popescu et al., 2009). Overall, the FTIR results revealed that the adsorbents exhibited a multitude of functional groups, which have the potential to play a role in the adsorption of Pb(II) and Cu(II). Furthermore, increasing the NaOH concentration in the activating reagent reduced the transmittance of functional groups, shown by the curve with a higher concentration of NaOH below the curve with a lower concentration of NaOH. In other words, increasing the NaOH concentration may result in an enhancement in the q_e of the adsorbent.

XRD analysis

The results of XRD analysis for TW, TW 0.2, TW 0.4, and TW 0.6 are shown in *Fig. 2*. As depicted in *Fig. 2*, the XRD patterns were utilized to assess the crystal structure and the impact of increasing NaOH concentration in the adsorbent activation. These adsorbents of TW, TW 0.2, TW 0.4, and TW 0.6 primarily consisted of cellulose, hemicellulose, and lignin. However, due to the presence of cellulose, the adsorbents consist of both crystalline and amorphous (non-crystalline) regions, with the non-crystalline portion primarily containing hemicellulose and lignin (Ma and Mu, 2010).

As shown in *Fig. 2*, it is evident that all the adsorbents exhibit a consistent trend. Initially, the adsorbents displayed distinct characteristic diffraction peaks at approximately 20.6°, with minor 2θ peaks at 15.4° and 34.7°, indicating the presence of cellulose crystal regions and a cellulose I-type crystal structure (Velásquez et al., 2016; Wen et al., 2017). *Fig. 2* also demonstrates a

slight increase in the crystallinity of the TW treated with the NaOH activating reagent. It may be due to the hydrolysis occurring in non-crystalline sections, particularly within hemicellulose and lignin (Wang et al., 2019).

Fig. 2. *The XRD for (a) TW, (b) TW 0.2, (c) TW 0.4 and (d) TW 0.6*

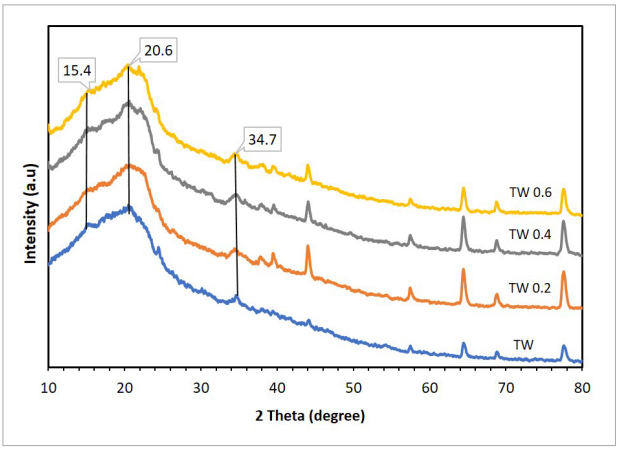

SEM analysis

Fig. 3 displays the SEM micrographs (500X) and the microstructural alterations in TW, TW 0.2, TW 0.4, and TW 0.6. The difference in surface characteristics between the TW adsorbent and the TW adsorbent activated with 0.2, 0.4, and 0.6 M NaOH can be clearly seen in *Fig. 3*.

TW showed a solid surface with the smooth texture and small pores with thick pore walls. Meanwhile, TW 0.2, TW 0.4, and TW 0.6 exhibited porous and dense structures with thinner pore walls. This suggests that a higher concentration of NaOH for activation resulted in the formation of a greater number of larger pores on the surface of TW. This phenomenon might involve the breakage of chemical bonds in proteins, cellulose, hemicellulose, and lignin, leading to the removal of these chemical compounds from the TW cell walls. This present finding is in line with a previous study indicating that the chemical compounds in okara can be removed through acid-base modification (Ullah et al., 2017). Furthermore, *Fig. 3*

Fig. 3. *The SEM for (a) TW, (b) TW 0.2, (c) TW 0.4 and (d) TW 0.6*

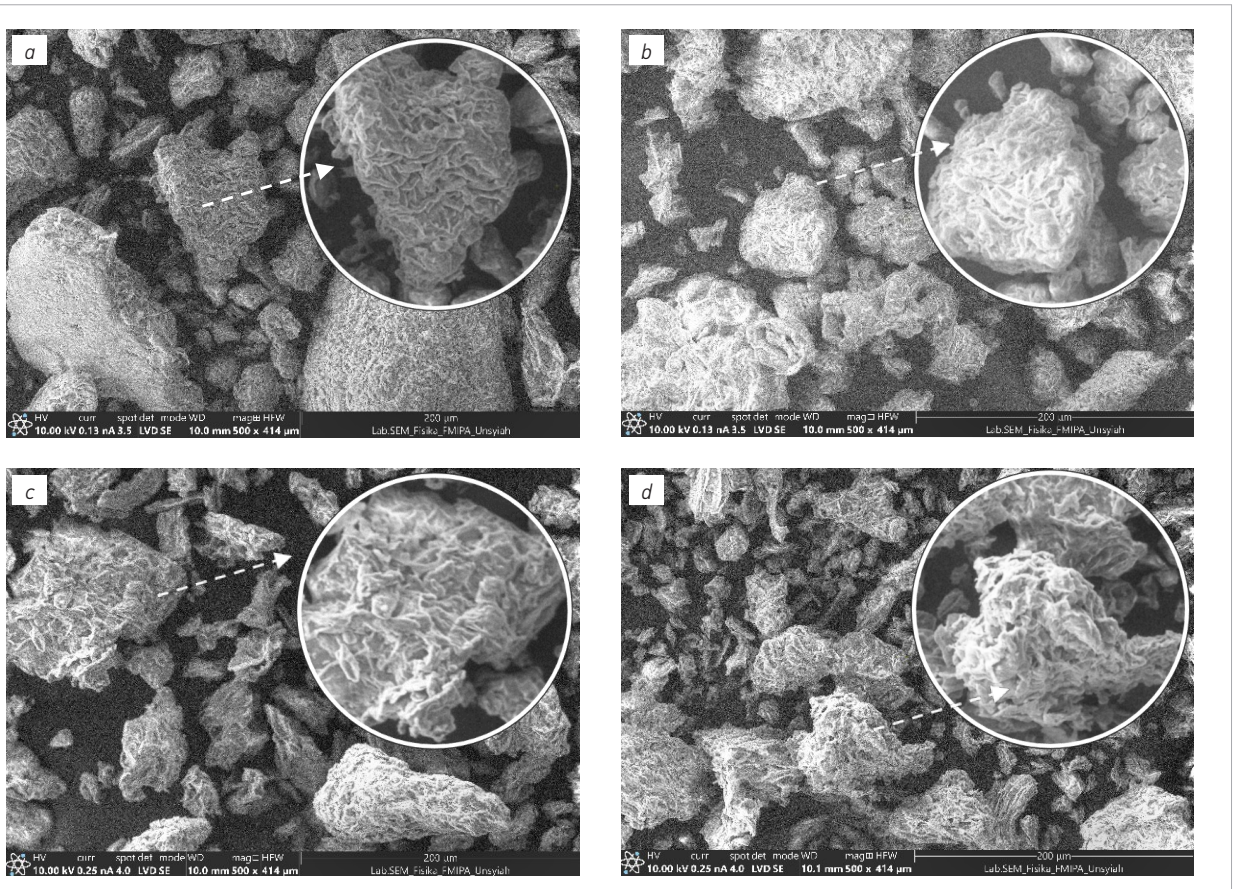

illustrates that the highest concentration of NaOH transformed the TW surface from a lumpy configuration into flakes that aggregated together, reduced the TW particle size, and generated more pores on the TW surface. This outcome might be reasonable since the NaOH treatment of the biosorbent results in surface ruptures and increased porosity (Iglaho et al., 2020).

Effect of contact time on adsorption capacity

The impact of contact time on the q for Pb(II) and Cu(II) using TW 0.6 at the C_0 was 499.51 and 499.92 mg/L, respectively, as shown in *Fig. 4*. Within the initial 10 min, the q increased significantly, reaching values of 99.76 mg/g and 87.81 mg/g, respectively. The initial 10-min contact time should represent the initial phase of the fast adsorption for the adsorbate onto the adsorbent. Typically, the initial phase of adsorption is governed by the diffusion of the adsorbate from the aqueous phase into the solid phase of the adsorbent (Medhi et al., 2020). Beyond this 10-min threshold, the change in the q was very small. The adsorption capacity of the adsorbent almost does not change after 10 min, and it stabilizes after 20 min. The intraparticle diffusion between the adsorbate and the biosorbent might be very slow after 20 min because most of the active sites get saturated, leading to a stabilization in the adsorption process. The intraparticle interactions are the form of Van der Waals forces, electrostatic attraction, and the presence of functional group bonds (Marlina et al., 2020). In this stage, the t_e of 40 min was chosen, and the q_e obtained was 99.86 mg/g and 87.83 for Pb(II) and Cu(II), respectively.

Effect of concentration of NaOH on adsorption capacity

Fig. 5 shows the effect of NaOH concentration on the q_e for Pb(II) and Cu(II). It appears that the influence of the increase in NaOH concentration on the q_e for Pb(II) is not significant. The increase in NaOH concentration from 0.2 M to 0.4 M resulted in only a 0.181% increase in the adsorption capacity of Pb(II), and for the increase in NaOH concentration from 0.2 M to 0.6 M, the adsorption capacity of Pb(II) increased by only 0.251%.

On the other hand, in Cu(II) adsorption, the rise in adsorption capacity is more pronounced than in Pb(II). The increase in NaOH concentration from 0.2 M to 0.4 M leads to a 4.924% boost in Pb(II) adsorption capacity, and an increase from 0.2 M to 0.6 M results in a 4.972% rise. This heightened adsorption capacity due to increased NaOH activator concentration aligns with findings from prior studies. Higher NaOH concentration releases more volatile matters, decreasing the transmittance of chemical functional groups. Consequently, more potential pores and adsorption surface area are formed, contributing to higher adsorption capacity (Muslim et al., 2007; Syahiddin and Muslim, 2018). As anticipated in the FTIR results, TW 0.6 exhibits the lowest transmittances for all chemical functional groups, leading to the highest adsorption capacity for Pb(II) and Cu(II).

Overall, the adsorption capacity for Pb(II) on the adsorbents is higher than Cu(II), as shown in *Fig. 5*. This trend is reasonable because the hydrated ionic radius of Pb(II) is 4.01 Å, which is smaller than that of Cu(II) ions, which is 4.19 Å leading to the better adsorption for Pb(II) compared

Fig. 4. *The q over contact time for Pb(II) and Cu(II) at the C_0 being 499.51 and 499.92 mg/L, respectively*

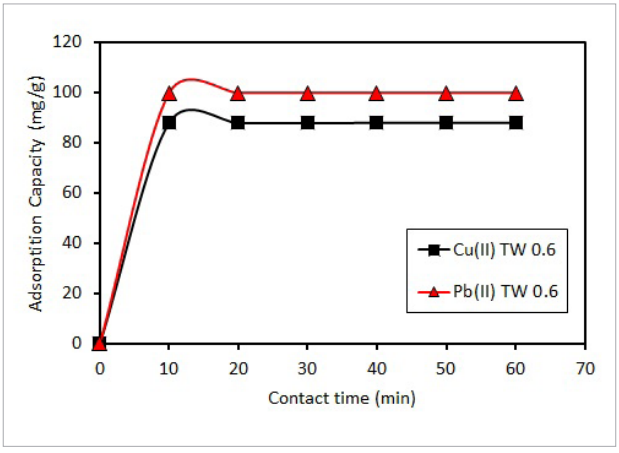

Fig. 5. *The q_e for Pb(II) and Cu(II) on various NaOH concentration at the C_0 being 499.51 and 499.92 mg/L, respectively*

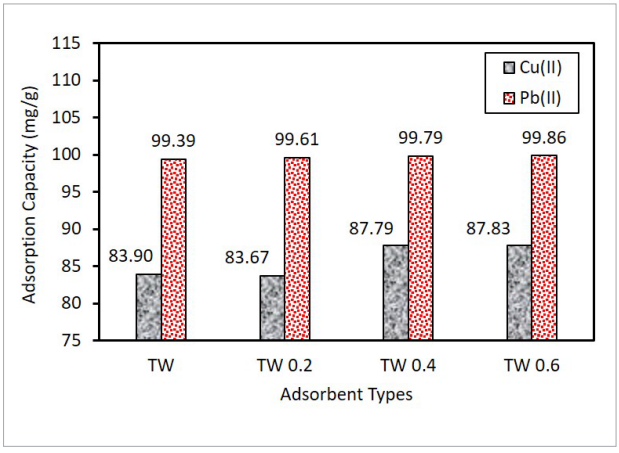

with Cu(II). The relation between hydrated radii of metal ions and adsorption affinity on adsorbents generally follows the trend that smaller hydrated radii correspond to stronger adsorption affinity (Goel et al., 2004). Smaller hydrated radii mean that metal ions have lower charge densities, making them easier to approach and interact with the adsorbent's surface (Dharmapriya et al., 2021).

Adsorption kinetic

In the adsorption kinetic study, there are only two adsorption plots using the TW 0.6 for Pb(II) and two adsorption plots for Cu(II) presented as examples. These plots correspond to the data shown in *Fig. 4*, which can be observed in *Fig. 6* and *Fig. 7*, respectively.

Fig. 6. *The adsorption kinetic of Pb(II) based on (a) LPFOK model and (b) LPSOK model for TW 0.6*

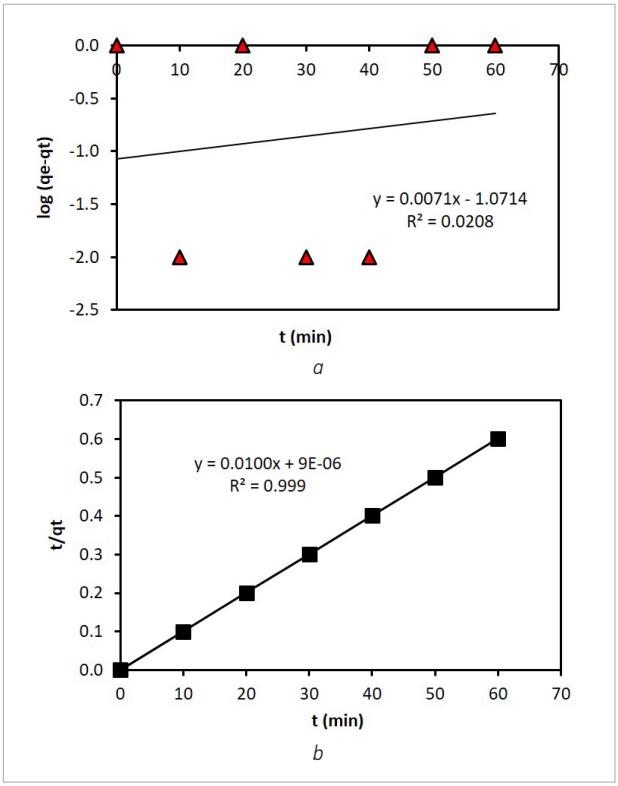

The adsorption kinetic parameters are summarized in *Tables 2* and *3* along with the fitting results of other adsorbents. As shown in *Figs. 6* and *7*, and *Tables 2* and *3*, both Pb(II) and Cu(II) adsorptions fitted very well in the LPSOK model. These results implied that both adsorbates took place on the surface of adsorbent (Robati, 2013). There should be chemical bonding between the adsorbates and

Fig. 7. *The adsorption kinetic of Cu(II) based on (a) LPFOK model and (b) LPSOK model for TW 0.6*

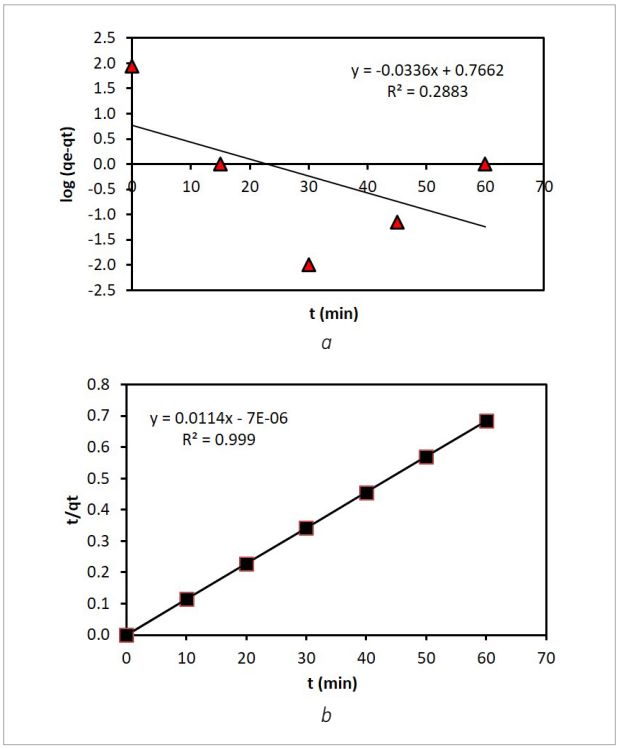

a multitude of functional groups on the surface of adsorbents, as described in the FTIR result. The rate-limiting step of Pb(II) and Cu(II) adsorption are chemisorption whereas the adsorption process of Pb(II) and Cu(II) are controlled by the chemical reaction between the adsorbates and the adsorbent surface (Emmanuel et al., 2020). As listed in *Table 2*, the Pb(II) adsorption capacity and the kinetic rate constant are identically not proportional to each other, and the rising NaOH concentration increased the speed of Pb(II) adsorption. In contrast, the Cu(II) adsorption capacity increased, the Cu(II) kinetic rate constant decreased, and the rising NaOH concentration decreased the speed of Cu(II) adsorption, as can be seen in *Table 3*. The speed of adsorption is directly proportional to the adsorption rate constant in the LPSOK model (Zhang, 2019). In addition, adsorption kinetics showed that the maximal adsorption capacity was achieved with TW 0.4 at the initial adsorbate concentration of 499.51 mg/L. However, to identify the most effective adsorbent in relation to adsorption capacity, adsorption tests should be conducted across a broad spectrum of initial adsorbate concentration. This challenge can be addressed by examining the overall adsorption capacity through an adsorption isotherm study (Chen et al., 2022).

Table 2. *The obtained constants of the Pb(II) adsorption kinetic*

	The Pb(II) LPFOK Model			The Pb(II) LPSOK Model		
	q_e	k_1	R^2	q_e	k_2	R^2
TW	2.813	0.060	0.266	99.005	0.442	0.999
TW 0.2	1.954	0.029	0.247	99.701	0.718	0.999
TW 0.4	8.472	0.0214	0.375	99.800	3.333	0.999
TW 0.6	0.085	0.0164	0.021	100.000	11.111	0.999

Table 3. *The obtained constants of the Cu(II) adsorption kinetic*

	The Cu(II) LPFOK Model			The Cu(II) LPSOK Model		
	q_e	k_1	R^2	q_e	k_2	R^2
TW	3.286	0.042	0.176	83.333	1.440	0.999
TW 0.2	3.307	0.065	0.293	83.333	0.720	0.999
TW 0.4	5.837	0.077	0.293	87.718	0.433	0.999
TW 0.6	3.896	0.021	0.288	87.719	0.001	0.999

Adsorption isotherm

Figs. 8 and *9* show a examples of the adsorption isotherm plots for Pb(II) and Cu(II), respectively, using TW 0.6 with the C_0 ranging within 9.89–499.51 mg/L and 10.08–499.92 mg/L, respectively. *Fig. 10(a)* and *Fig. 10(b)* display an example of the adsorption isotherm plots based on the LBETAI model for both Pb(II) and Cu(II). *Fig. 10(a)* and *Fig. 10(b)* show the LBETAI plot for Pb(II) and Cu(II) at the same range of initial adsorbate concentration. The adsorption isotherm results for all the adsorbents are listed in *Table 4*.

Fig. 8. *The adsorption isotherm of Pb(II) based on (a) LLAI model and (b) LFAI model using TW 0.6*

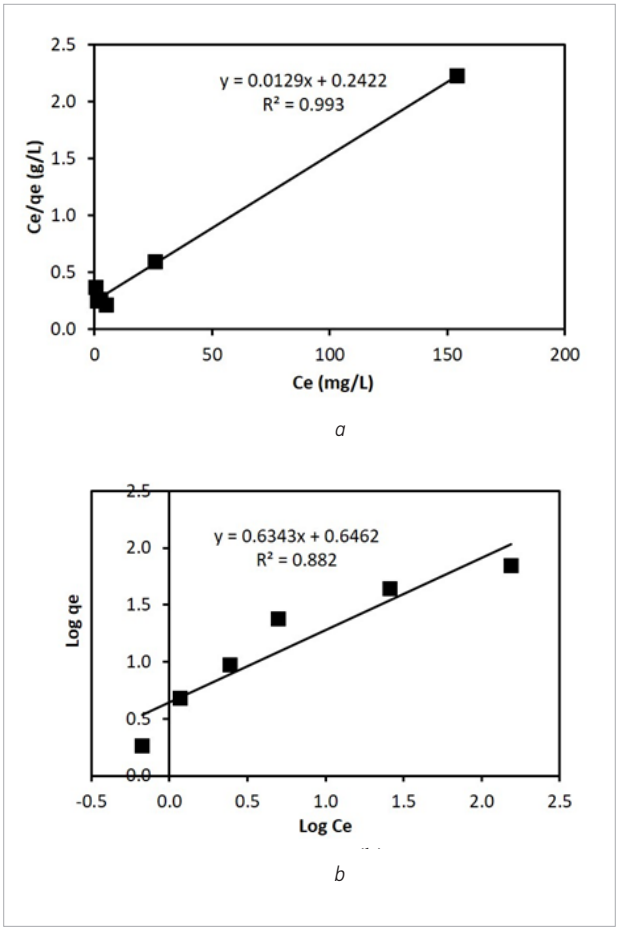

Fig. 9. *The adsorption isotherm of Cu(II) based on (a) LLAI model and (b) LFAI model using TW 0.6*

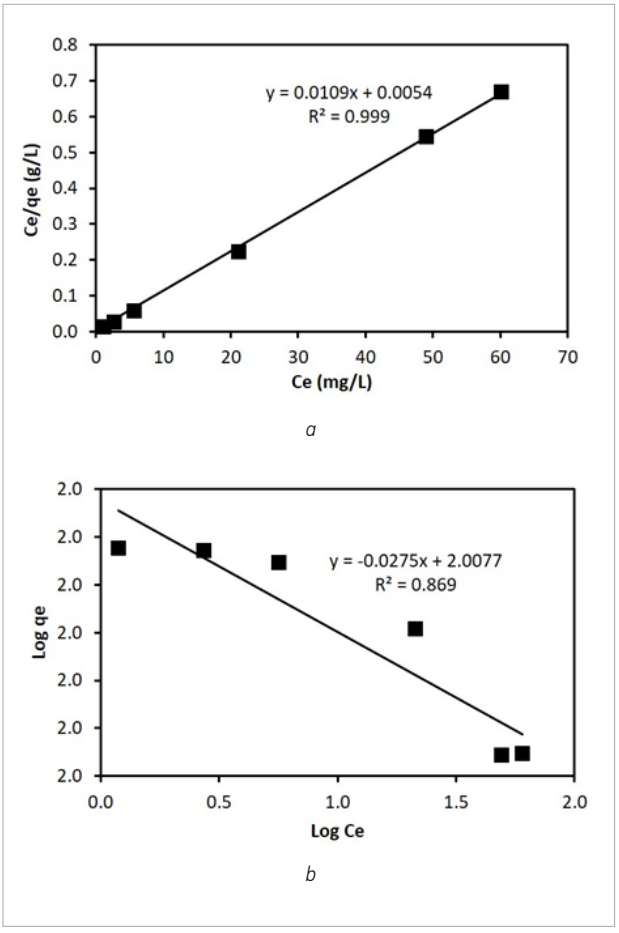

Fig. 10. *The adsorption isotherm based for LBETAI model for (a) Pb(II) and (b) Cu(II) using TW 0.6*

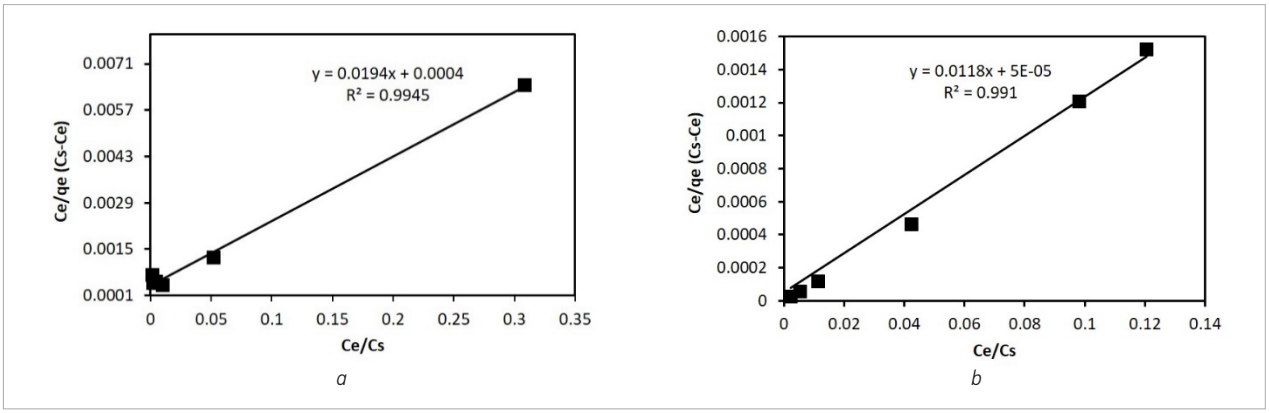

Based on *Figs. 8* and *9*, as well as *Table 4*, the Langmuir isotherm yielded the best fit, with average R^2 values of 0.939 and 0.988 for Pb(II) and Cu(II), respectively. Meanwhile, the average R2 values for the Freundlich isotherm were 0.772 and 0.735, respectively. Due to the negative n value of Cu(II), the Freundlich isotherm may not be the most suitable model for describing the adsorption behavior. Additionally, the Langmuir isotherm proved to be reasonable in this case because the adsorbate monolayer on the adsorbent surface is generally associated with pseudo-second-order kinetic adsorption (Muslim, 2017; Islam et al., 2021), which aligns with the LPSOK result discussed earlier. Meanwhile, the average R^2 values for the Freundlich isotherm were 0.772 and 0.735, respectively. Due to the negative n value of Cu(II), the Freundlich isotherm may not be the

Table 4. *The obtained constants of the Pb(II) and Cu(II) adsorption isotherm*

Model	Adsorbate	Parameter	Adsorbent			
			TW	TW 0.2	TW 0.4	TW 0.6
LLAI	Pb(II)	R^2	0.931	0.932	0.902	0.993
		q_m (mg/g)	59.172	72.993	76.336	77.519
		K_L (L/mg)	0.021	0.038	0.029	0.053
	Cu(II)	R^2	0.961	0.994	0.998	0.999
		q_m (mg/g)	68.027	86.956	90.090	91.743
		K_L (L/mg)	0.071	0.797	1.521	2.019
LFAI	Pb(II)	R^2	0.709	0.722	0.775	0.882
		n	1.515	1.626	1.605	1.577
		K_F (L/mg)	2.042	3.969	3.435	4.428
	Cu(II)	R^2	0.801	0.837	0.434	0.869
		n	-6.978	-24.449	-39.525	-36.363
		K_F (L/mg)	147.231	105.123	99.197	101.788
LBETAI	Pb(II)	R^2	0.969	0.968	0.956	0.995
		qs (mg/g)	25.126	42.553	45.662	50.505
		CBET (L/mg)	36.182	39.167	27.375	49.500
	Cu(II)	R^2	0.849	0.972	0.988	0.991
		qs (mg/g)	48.077	76.923	81.433	84.388
		CBET (L/mg)	41.600	130.000	153.500	237.000

most suitable model for describing the adsorption behavior. Additionally, the Langmuir isotherm proved to be reasonable in this case because the adsorbate monolayer on the adsorbent surface is generally associated with pseudo-second-order kinetic adsorption (Muslim, 2017; Islam et al., 2021), which aligns with the LPSOK result discussed earlier.

As anticipated from the FTIR results, the influence of NaOH concentration on the adsorption capacity of Pb(II) and Cu(II) is clearly demonstrated in *Table 2*. The adsorption capacity exhibited a noticeable increase with the rise in NaOH concentration, which is in line with the increase in total pore volume (Kovo et al., 2015). Consequently, TW 0.6 exhibited the highest adsorption capacity for Pb(II) and Cu(II), with respective overall capacities of 77.519 mg/g and 91.734 mg/g. The total pore volume for TW 0.6 was measured at 0.053 L/mg for Pb(II) and 2.019 L/mg for Cu(II). Additionally, the BET adsorption isotherm underscored this upward trend, revealing saturation capacities and total pore volumes of 50.505 mg/g and 49.500 L/mg for Pb(II), and 84.388 mg/g and 237.000 L/mg for Cu(II).

Conclusions

The study focuses on creating an adsorbent from tofu waste (TW) to remove Pb(II) and Cu(II). Higher NaOH concentrations were found to enhance the adsorption capacity of tofu waste (TW). XRD analysis showed increased crystallinity post NaOH treatment, identifying cellulose, hemicellulose, and lignin in the adsorbent. SEM analysis revealed larger pores with higher NaOH concentrations, leading to a reduction in adsorbent size. Optimal adsorption occurred in 40 mins, reaching 99.86 mg/g and 87.81 mg/g for Pb(II) and Cu(II) using TW activated by 0.6 M NaOH. Pseudo second-order kinetics model fit well, with Langmuir isotherm showing the best fit for adsorption with a maximum overall adsorption capacity of 77.519 mg/g and 91.743 mg/g, respectively. BET study indicated saturation capacities and total pore volumes of 50.505 mg/g and 49.500 L/mg, respectively, for Pb(II), and 84.388 mg/g and 237.000 L/mg, respectively, for Cu(II).

Acknowledgments

The authors would like to express their sincere gratitude to the Postgraduate School of Engineering Studies at Universitas Syiah Kuala for their invaluable technical support in the experimental work.

Disclosure Statement

We declare that we have no known financial or interpersonal conflicts that would have an impact on the research presented in this study. We are not connected to or a part of any group or organization that has a financial or non-financial stake in the topics or materials covered in this manuscript.

References

Al-Harby NF, Albahly EF, Mohamed NA. (2021) Kinetics, Isotherm and Thermodynamic Studies for Efficient Adsorption of Congo Red Dye from Aqueous Solution onto Novel Cyanoguanidine-Modified Chitosan Adsorbent. Polymers (Basel) 13(24): 4446. Available at: https://doi.org/10.3390/polym13244446

Ali H., Khan E., Ilahi I. (2019) Environmental chemistry and ecotoxicology of hazardous heavy metals: environmental persistence, toxicity, and bioaccumulation. Journal of Chemistry 2019: 6730305. Available at: https://doi.org/10.1155/2019/6730305

André L.C., Alexandro M.M.V., Eurica M.N., Marcos H.K., Marcos R.G., Alessandro C.M., Tais L.S., Juliana C.G.M., Vitor C.A. (2011) NaOH-activated carbon of high surface area produced from coconut shell: Kinetics and equilibrium studies from the methylene blue adsorption. Chemical Engineering Journal 174(1): 117-125. Available at: https://doi.org/10.1016/j.cej.2011.08.058

Basu M., Guha A.K., Ray L. (2017) Adsorption of Lead on Cucumber Peel. Journal of Cleaner Production 151: 603-615. Available at: https://doi.org/10.1016/j.jclepro.2017.03.028

Bentley F.F., Smithson L.D., Rozek A.L. (1968) Infrared Spectra and Characteristic Frequencies ~ 700-300 cm-1, Interscience, New York.

Biao G., Hong F., Chong C., Chong-Jian J., Fan X., Ying L. (2013) Heavy Metal Concentrations in Soil and Agricultural Products Near an Industrial District. Polish Journal of Environmental Studies 22(5): 1357-1362. Available at: http://www.pjoes.com/Heavy-Metal-Concentrations-in-Soil-r-nand-Agricultural-Products-Near-r-nan-Industrial,89099,0,2.html.

Biswajit S., Sudip K.D. (2013) Adsorptive removal of Cu(II) from aqueous solution and industrial effluent using natural/ wastes. Colloids and Surfaces B: Biointerfaces 107: 97-106. Available at: https://doi.org/10.1016/j.colsurfb.2013.01.060

Blázquez G., M.A. Martín-Lara M.A., Tenorio G., Calero M. (2011) Batch biosorption of lead(II) from aqueous solutions by olive tree pruning waste: Equilibrium, kinetics and thermodynamic study. Chemical Engineering Journal 168(1): 170-177. Available at: https://doi.org/10.1016/j.cej.2010.12.059

Chakravarty P., Sarma N.S., Sarma H.P. (2010) Removal of Lead(II) from Aqueous Solution Using Heartwood of Areca Catechu Powder. Desalination 256(1-3): 16-21. Available at: https://doi.org/10.1016/j.desal.2010.02.029

Chen X., Hossain Md. F., Duan C., Lu, J., Tsang Y. F., Islam Md. S., Zhou Y. (2022) Isotherm models for adsorption of heavy metals from water - A review. Chemosphere 307(1): 135545. Available at: https://doi.org/10.1016/j.chemosphere.2022.135545

Dancila A.M., Orbulet O.D., Modrogan C., Caprarescu S. (2019) Soybean waste material as potential adsorbent or heavy metal ions from aqueous solutions. International Multidisciplinary Scientific GeoConference 19(5.2): 823-830. Available at: https://doi.org/10.5593/sgem2019/5.2/S20.103

Dharmapriya T.N., Li D., Chung Y.C., Huang P.J. (2021) Green Synthesis of Reusable Adsorbents for the Removal of Heavy Metal Ions. ACS Omega 6(45): 30478-30487. Available at: https://doi.org/10.1021/acsomega.1c03879

Dharsana M., Josej P.A. (2022) Adsorption of lead from contaminated water using biosorbent. Materials and Technology 56(2): 171-177. Available at: https://doi.org/10.17222/mit.2021.352

Ebrahimi M., Khalili N., Razi S. (2020) Keshavarz-Fathi M, Khalili N, Rezaei N. Effects of lead and cadmium on the immune system and cancer progression. Journal of Environmental Health Science and Engineering 18(1): 335-343. Available at: https://doi.org/10.1007/s40201-020-00455-2

Emmanuel D.R., Fortela L.D., Wayne S., Rafael H., Mark E.Z., (2020) Adsorption kinetic modeling using pseudo-first order and pseudo-second order rate laws: A review. Cleaner Engineering and Technology 1: 100032. Available at: https://doi.org/10.1016/j.clet.2020.100032

Fahma F., Iwamoto S., Hori N., Iwata T., Takemura A. (2011) Effect of pre-acid-hydrolysis treatment on morphology and properties of cellulose nanowhiskers from coconut husk. Cellulose 18(2): 443-450. Available at: https://doi.org/10.1007/s10570-010-9480-0

Foggia M.D., Taddei P., Torreggiani A., Dettin M., Tinti (2011) Self-assembling peptides for biomedical applications: Ir and raman spectroscopies for the study of secondary structure. Proteomics Research Journal 2(3): 231-272. Available at: https://hdl.handle.net/11585/400363

Foo K.Y., Hameed B.H. (2010) Insights into the modeling of adsorption isotherm systems. Chemical Engineering Journal 156: 2-10. Available at: https://doi.org/10.1016/j.cej.2009.09.013

Fotsing P.N., Woumfo E.D., Măicăneanu S.A., Vieillard J., Tcheka C., Ngueagni P.T., Siéwé J.M. (2020) Removal of Cu (II) from aqueous solution using a composite made from cocoa cortex and sodium alginate. Environmental Science and Pollution Research 27: 8451-8466. Available at: https://doi.org/10.1007/s11356-019-07206-3

Fu F., Wang Q. (2011) Removal of heavy metal ions from wastewaters: a review. Journal of Environmental Management 92(3): 407-418. Available at: https://doi.org/10.1016/j.jenvman.2010.11.011

Geng Z., Lin Y., Yu X., Shen Q., Ma L., Li Z., Pan N., Wang X. (2012) Highly efficient dyeadsorption and removal: a functional hybrid of reduced graphene oxide-Fe3O4nanoparticles as an easily regenerative adsorbent. Journal of Materials Chemistry 22: 3527. Available at: https://doi.org/10.1039/c2jm15544c

Goel J., Kadirvelu K., Rajagopal C. (2004) Competitive Sorption of Cu(II), Pb(II) and Hg(II) Ions from Aqueous Solution Using Coconut Shell-Based Activated Carbon. Adsorption Science and Technology 22(3): 257-273. Available at: https://doi.org/10.1260/0263617041503453

Grand View Research (2019) GVR Report coverTofu Market Size, Share and Trends Report.

Tofu Market Size, Share and Trends Analysis Report By Distribution Channel (Supermarkets and Hypermarkets, Grocery Stores, Online, Specialty Stores), By Region, And Segment Forecasts, 2019 - 2025. Available at: https://www.grandviewresearch.com/industry-analysis/tofu-market.

Hafizuddin M.S., Lee C.L., Chin K.L., H'ng P.S., Khoo P.S., Rashid U. (2021) Fabrication of Highly Microporous Structure Activated Carbon via Surface Modification with Sodium Hydroxide. Polymers (Basel) 13(22): 3954. PMID: 34833252. Available at: https://doi.org/10.3390/polym13223954

Hesas R.H., Daud W. M. A., Sahu J.N., Arami-Niya A. (2013) The effects of a microwave heating method on the production of activated carbon from agricultural waste: A review. Journal of Analytical and Applied Pyrolysis 100: 1-11. Available at: https://doi.org/10.1016/j.jaap.2012.12.019

Ho Y.S., Wase D.A.J., Forster C.F. (1996) Kinetic studies of competitive heavy metal adsorption by sphagnum moss peat. Environmental Technology 17: 71-77. Available at: https://doi.org/10.1080/09593331708616362

Ho Y.S. (2003) Removal of copper ions from aqueous solution by tree fern. Water Research 37: 2323-2330. https://doi.org/10.1016/S0043-1354(03)00002-2

Hossain M.A., Ngo H.H., Guo W.S., Nguyen T.V. (2012) Palm oil fruit shells as biosorbent for copper removal from water and wastewater: Experiments and sorption models. Bioresource Technology 113: 97-101. Available at: https://doi.org/10.1016/j.biortech.2011.11.111

Ighalo J.O., Adeniyi A.G. (2020) A mini-review of the morphological properties of biosorbents derived from plant leaves. SN Applied Sciences 2: 509. Available at: https://doi.org/10.1007/s42452-020-2335-x

Inam M.A., Khan R., Akram M., Khan S., Park D.R., Yeom I.T. (2019) Interaction of Arsenic Species with Organic Ligands: Competitive Removal from Water by Coagulation-Flocculation-Sedimentation (C/F/S). Molecules 24(8): 1619. Available at: https://doi.org/10.3390/molecules24081619

Ifijen I.H., Itua A.B., Maliki M., Ize-Iyamu C.O., Omorogbe S.O., Aigbodion A.I., Ikhuoria E.U. (2020) The removal of nickel and lead ions from aqueous solutions using green synthesized silica microparticles. Heliyon 6(9): e04907. Available at: https://doi.org/10.1016/j.heliyon.2020.e04907

Islam Md. A., Chowdhury M. A., Mozumder Md. S. I., Md. Tamez Uddin Md. T. (2021) Langmuir Adsorption Kinetics in Liquid Media: Interface Reaction Model. ACS Omega 6(22): 14481-14492. Available at: https://doi.org/10.1021/acsomega.1c01449

Jiménez S., Andreozzi M., Micó M.M., Álvarez M.G., Contreras S. (2019) Produced water treatment by advanced oxidation processes. Science of The Total Environment 66: 12-21. Available at: https://doi.org/10.1016/j.scitotenv.2019.02.128

Jomova K., Makova M., Alomar S.Y., Alwasel S.H., Nepovimova E., Kuca K., Rhodes C.J., Valko M. (2022) Essential metals in health and disease. Chemico-Biological Interactions 367: 110173. Available at: https://doi.org/10.1016/j.cbi.2022.110173

Kampalanonwat P., Supaphol P. (2014) The study of competitive adsorption of heavy metal ions from aqueous solution by aminated polyacrylonitrile nanofiber mats. Energy Procedia 56: 143. Available at: https://doi.org/10.1016/j.egypro.2014.07.142

Kaur M., Kumari S., Sharma P. (2020) Removal of Pb(II) from aqueous solution using nanoadsorbent of Oryza sativa husk: Isotherm, kinetic and thermodynamic studies. Biotechnology Reports 25: e00410. Available at: https://doi.org/10.1016/j.btre.2019.e00410

Khan A., Khan S., Khan M.A., Qamar Z., Waqas M. (2015) The uptake and bioaccumulation of heavy metals by food plants, their effects on plants nutrients, and associated health risk: a review. Environmental Science and Pollution Research 22(18): 13772-13799. Available at: https://doi.org/10.1007/s11356-015-4881-0

Khayyun T.S., Mseer A.H. (2019) Comparison of the experimental results with the Langmuir and Freundlich models for copper removal on limestone adsorbent. Applied Water Science 9: 170. Available at: https://doi.org/10.1007/s13201-019-1061-2

Kovo G. A., Folasegun A. D., Kayode O. A. (2015) Mechanism on the sorption of heavy metals from binary-solution by a low cost montmorillonite and its desorption potential. Alexandria Engineering Journal 54(3): 757-767. Available at: https://doi.org/10.1016/j.aej.2015.03.025

Kumar P.G.V.S.R., Malla K., Yerra B., Rao K.S, (2019) Removal of Cu(II) using three low-cost adsorbents and prediction of adsorption using artificial neural networks. Applied Water Science (9): 44. Available at: https://doi.org/10.1007/s13201-019-0924-x

Kumar S., Verma T., Mukherjee R., Ariese F., Somasundaram K., Umapathy S. (2016) Raman and infrared microspectroscopy: Towards quantitative evaluation for clinical research by ratiometric analysis. Chemical Society Reviews 45: 1879-1900. Available at: https://doi.org/10.1039/C5CS00540J

Kurniawan T.A., Chan G.Y.S., Wai-Hung L., Babel S. (2006) Physico-chemical treatment techniques for wastewater laden with heavy metals. Chemical Engineering Journal 118(1-2): 1385-8947. Available at: https://doi.org/10.1016/j.cej.2006.01.015

Lagergren, S. (1989) About the theory of so-called adsorption of soluble substances. Kungliga Svenska Vetenskapsakademies Handlingar 24: 1-39.

Lee J.J., Cha J.H., Aim R.B., Han K.B., Kim C.W. (2008) Fiber filter as an alternative to the process of flocculation-sedimentation for water treatment. Desalination 231(1-3): 323-331. Available at: https://doi.org/10.1016/j.desal.2007.11.051

Lelièvre P., Sancey L., Coll J.-L., Deniaud A., Busser B. (2020) Multifaceted Roles of Copper in Cancer: A Trace Metal Element with Dysregulated Metabolism, but Also a Target or a Bullet for Therapy. Cancers 12: 3594. Available at: https://doi.org/10.3390/cancers12123594

Li J, Dong X, Liu X, Xu X, Duan W, Park J, Gao L, Lu Y. (2022) Comparative Study on the Adsorption Characteristics of Heavy Metal Ions by Activated Carbon and Selected Natural Adsorbents. Sustainability 14(23): 15579. Available at: https://doi.org/10.3390/su142315579

Ma M.M., Mu T.H. (2016) Effects of extraction methods and particle size distribution on the structural, physicochemical, and functional properties of dietary fiber from deoiled cumin. Food chemistry 194: 237-246. Available at: https://doi.org/10.1016/j.foodchem.2015.07.095

Mansour S.A., Tony M.A., Tayeb A.M. (2019) Photocatalytic performance and photodegradation kinetics of Fenton-like process based on haematite nanocrystals for basic dye removal. Springer Nature Applied Sciences 1: 265. Available at: https://doi.org/10.1007/s42452-019-0286-x

Marlina, Iqhrammullah M., Saleha S., Fathurrahmi, Maulina F.P., Idroes R. (2020) Polyurethane film prepared from ball-milled algal polyol particle and activated carbon filler for NH3-N removal. Heliyon 6(8): e04590. Available at: https://doi.org/10.1016/j.heliyon.2020.e04590

Mashhadimoslem H., Maleki F., Khosrowshahi M.S. (2024) Chapter 10 - Modeling of polymeric adsorbent behavior, Editor(s): Ahad Ghaemi, Reza Norouzbeigi, Hadiseh Masoumi. Polymeric Adsorbents, 393-432. Available at: https://doi.org/10.1016/B978-0-323-99746-1.00010-0

Maximize Market Research (2023) Tofu Market: Global Industry Analysis and Forecast (2023-2029). Available at: https://www.maximizemarketresearch.com/market-report/global-tofu-market/111769/.

Milićević S., Vlahović M., Kragović M., Martinović S., Milošević V., Jovanović I., Stojmenović M. (2020) Removal of Copper from Mining Wastewater Using Natural Raw Material-Comparative Study between the Synthetic and Natural Wastewater Samples. Minerals 10(9): 753. Available at: https://doi.org/10.3390/min10090753

Mok W.K., Tan Y.X., Lee J., Kim J., Chen W.N. (2019). A metabolomic approach to understand the solid-state fermentation of okara using Bacillus subtilis WX-17 for enhanced nutritional profile. AMB Express 9(1): 60. Available at: https://doi.org/10.1186/s13568-019-0786-5

Mondragon G., Fernandes S., Retegi A., Peña C., Algar I., Eceiza A., Arbelaiz, A. (2014) A common strategy to extracting cellulose nanoentities from different plants. Industrial Crops and Products 55: 140-148. Available at: https://doi.org/10.1016/j.indcrop.2014.02.014

Murphy O.P., Vashishtha M., Palanisamy P., and K. Vasanth Kumar K.V., (2023) A Review on the Adsorption Isotherms and Design Calculations for the Optimization of Adsorbent Mass and Contact Time. ACS Omega 8(20): 17407-17430. Available at: https://doi.org/10.1021/acsomega.2c08155

Muslim A. (2017) Australian Pine Cones-Based Activated Carbon for Adsorption of Copper in Aqueous Solution. Journal of Engineering Science and Technology 12(2): 280-295.

Muslim A., Abubakar, Alam P.N., Usman H., Randa G., Widayat A.H., Al Hakim A.Y., Hadibarata T. (2022) Silicified coal adsorbents for adsorption of Cu(II) from the aqueous Solution: Non-Linear kinetic and isotherm studies. Materials Today: Proceedings 63(1): S400-S405. Available at: https://doi.org/10.1016/j.matpr.2022.03.556

Muslim A., Aprilia S., Suha T.A., Fitri, Z. (2017) Adsorption of Pb(II) ions from Aqueous Solution Using Activated Carbon Prepared from Areca Catechu Shell: Kinetic, Isotherm and Thermodynamic Studies. Journal of the Korean Chemical Society 61(3): 89-96, 1017-2548. Available at: https://doi.org/10.5012/jkcs.2017.61.3.89.

Muslim A., Thaib A., Rosnelly C.M., Hidayatullah M., Riyadh M., Guswara F.Y., Kadri A. (2021) Musa Acuminata Banana Bunch-Based Activated Carbon for Adsorption of Cu(II) Ions in Aqueous Solution: Kinetic and Isotherm Studies. Iranian Journal of Chemistry and Chemical Engineering (IJCCE) 10(5): 1522-1532. Available at: https://doi.org/10.30492/IJCCE.2020.43316.

Nguyen H.T., Pham T.T. (2023) Brilliant Green Biosorption from Aqueous Solutions on Okara: Equilibrium, Kinetic and Thermodynamic Studies. Journal of Water and Environment Technology 21(1): 30-40. Available at: https://doi.org/10.2965/jwet.22-059

Obulapuram P.K., Arfin T., Mohammad F., Khiste S.K., Chavali M., Albalawi A.N., Al-Lohedan H.A. (2021) Adsorption, Equilibrium Isotherm, and Thermodynamic Studies towards the Removal of Reactive Orange 16 Dye Using Cu(I)-Polyaninile Composite. Polymers (Basel) 13(20): 3490. Available at: https://doi.org/10.3390/polym13203490

Perwitasari D.S., Pracesa Y.A.Y., Pangestu M.A., Tol, P.S. (2021) Langmuir and Freundlich isotherm approximation on adsorption. NST Proceeding of the 2nd International Conference Eco-Innovation in Science, Engineering, and Technology. Available at: http://dx.doi.org/10.11594/nstp.2021.1417.

Popescu C.M., Singurel G., Popescu M.C., Vasile C., Argyropoulos D,S,, Willfor S. (2009) Vibrational spectroscopy and X-ray diffraction methods to establish the differences between hardwood and softwood. Carbohydrate Polymers 77(4): 851-857. Available at: https://doi.org/10.1016/j.carbpol.2009.03.011

Popescu M., Popescu M.C., Singurel G., Vasile C., Argyropoulos D.S., Willfor S. (2007) Spectral Characterization of Eucalyptus Wood. Applied Spectroscopy 61(11): 1168-1177. Available at: https://doi.org/10.1366/000370207782597076

Quist-Jensen C.A., Macedonio F., Drioli E. (2015) Membrane technology for water production in agriculture: Desalination and wastewater reuse. Desalination 364: 17-32. Available at: https://doi.org/10.1016/j.desal.2015.03.001

Ren B., Shahzad M.K., Zhang X., Jin Y., Ouyang F., Li H. (2018) Fermented Corn Stalk for Biosorption of Copper. https://doi.org/10.1155/2018/8989053

(II) from Aqueous Solution. Advances in Materials Science and Engineering 2018: 8989053. Available at: https://doi.org/10.1155/2018/8989053

Revellame E.D., Fortela D.L., Sharp W., Hernandez R., Zappi M.E. (2020) Adsorption kinetic modeling using pseudo-first order and pseudo-second order rate laws: A review. Cleaner Engineering and Technology 1: 100032. Available at: https://doi.org/10.1016/j.clet.2020.100032

Robati D. (2013) Pseudo-second-order kinetic equations for modeling adsorption systems for removal of lead ions using multi-walled carbon nanotube. Journal of Nanostructure in Chemistry 3: 55. Available at: https://doi.org/10.1186/2193-8865-3-55

Sabela M.I., Kunene K., Kanchi S., Xhakaza N.M, Bathinapatla A., Mdluli P., Sharma D., Krishna B.K. (2019) Removal of copper (II) from wastewater using green vegetable waste derived activated carbon: An approach to equilibrium and kinetic study. Arabian Journal of Chemistry 12: 4331-4339. Available at: https://doi.org/10.1016/j.arabjc.2016.06.001

Samieym B., Cheng C.H., Wu J. (2014) Organic-Inorganic Hybrid Polymers as Adsorbents for Removal of Heavy Metal Ions from Solutions: A Review. Materials 7(2): 673-726. https://doi.org/10.3390/ma7020673

Sha T., Liu J., Sun M., Li L., Bai J., Hu Z., Zhou M. (2019) Green and lowcost synthesis of nitrogen-doped graphene-like mesoporous nanosheets from the biomass waste of okara for the amperometric detection of vitamin C in real samples. Talanta 200: 300,306. https://doi.org/10.1016/j.talanta.2019.03.071

Syahiddin D.S., Muslim A. (2018) Adsorption of Cu(II) Ions onto Myristica Fragrans Shell-based Activated Carbon: Isotherm, Ki-

netic and Thermodynamic Studies. Journal of the Korean Chemical Society 62: 79-86. http://dx.doi.org/10.5012/jkcs.2018.62.2.79

Ullah I., Yin T., Xiong S., Zhang J., Zu D., Zhang M. (2017) Structural characteristics and physicochemical properties of okara (soybean residue) insoluble dietary fiber modified by high-energy wet media milling. LWT - Food Science and Technology 82: 15-22. Available at: https://doi.org/10.1016/j.lwt.2017.04.014

Velásquez C.J., Gañán P., Posada P., Castro C., Serpa A., Gómez H.C., Putaux J.L., Zuluaga R.R, Zuluaga (2016) Influence of combined mechanical treatments on the morphology and structure of cellulose nanofibrils: Thermal and properties of the resulting films. Industrial Crops and Products 85: 1-10. Available at: https://doi.org/10.1016/j.indcrop.2016.02.036

Vorontsov A.V. (2019) Advancing Fenton and photo-Fenton water treatment through the catalyst design. Journal of Hazardous Materials 372: 103-112. Available at: https://doi.org/10.1016/j.jhazmat.2018.04.033

Wang Z., Qu L., Qian J., He Z., Yi S. (2019) Effects of the ultrasound-assisted pretreatments using borax and sodium hydroxide on the physicochemical properties of Chinese fir. Ultrasonics Sonochemistry 50: 200-207. Available at: https://doi.org/10.1016/j.ultsonch.2018.09.017

Wen Y., Niu M., Zhang B.J., Zhao S.M., Xiong S.B. (2017) Structural characteristics and functional properties of rice bran dietary fiber modified by enzymatic and enzyme-micronization treatments. LWT-Food Science and Technology 75: 344-351. Available at: https://doi.org/10.1016/j.lwt.2016.09.012

Xiang Z., Gao W., Chen L., Lan W., Zhu J., Runge T. (2016) A comparison of cellulose nanofibrils produced from Cladophora glomerata algae and bleached eucalyptus pulp. Cellulose 23(1): 493-503. Available at: https://doi.org/10.1007/s10570-015-0840-7

Yang T., Liu T.X, Li X.T, Tang C.H. (2019) Novel nanoparticles from insoluble soybean polysaccharides of okara as unique pickering stabilizers for oil-in-water emulsions. Food Hydrocoll 94: 255-267. Available at: https://doi.org/10.1016/j.foodhyd.2019.03.035

Yargıc A.S., Sahin R.Z.Y., Özbay N., Önal E. (2015) Assessment of toxic copper (II) biosorption from aqueous solution by chemically-treated tomato waste. Journal of Cleaner Production 88: 152-159. Available at: https://doi.org/10.1016/j.jclepro.2014.05.087

Yu C.A, Yang C.Y. (2019) Bio-ionic liquid pretreatment and ultrasoundpromoted enzymatic hydrolysis of black soybean okara. Journal of Bioscience and Bioengineering 127: 767-773. Available at: https://doi.org/10.1016/j.jbiosc.2018.12.007

Zein R., Hidayat D.A., Elfia M., Nazarudin N, Munaf E. (2014) Sugar palm Arenga pinnata Merr (Magnoliophta) fruit shell as biomaterial to remove Cr(III), Cr(VI), Cd(II) and Zn(II) from aqueous solution. Journal of Water Supply: Research and Technonoly-AQUA 63(7): 553-559. Available at: https://doi.org/10.2166/aqua.2014.120

Zhang J. (2019) Physical insights into kinetic models of adsorption. Separation and Purification Technology 229: 115832. Available at: https://doi.org/10.1016/j.seppur.2019.115832

This article is an Open Access article distributed under the terms and conditions of the Creative Commons Attribution 4.0 (CC BY 4.0) License (http://creativecommons.org/licenses/by/4.0/).